ACS OMEGA

http://pubs.acs.org/journal/acsodf

Article

A Promising Three-Step Heat Treatment Process for Preparing CuO Films for Photocatalytic Hydrogen Evolution from Water

Pannan I. Kyesmen,* Nolwazi Nombona, and Mmantsae Diale*

Cite This: *ACS Omega* 2021, 6, 33398−33408

Read Online

ACCESS | Metrics & More | Article Recommendations | Supporting Information

ABSTRACT: Copper (II) oxide (CuO) nanostructures were prepared on fluorine-doped tin oxide (FTO) using a three-step heat treatment process in a sol−gel dip-coating method. The precursor used for the dip-coating process was prepared using copper acetate, propan-2-ol, diethanolamine, and polyethylene glycol 400. Dip-coated films in layers of 2, 4, 6, 8, and 10 were prepared by drying each layer at 110 and 250 °C for 10 and 5 min, respectively, followed by calcination at 550 °C for 1 h. The films were applied toward photocatalytic hydrogen evolution from water. The X-ray diffraction (XRD) pattern of the films confirmed the tenorite phase of pure CuO. Raman spectroscopy revealed the $1A_g$ and $2B_g$ phonon modes of CuO, confirming the high purity of the films produced. The CuO films absorb significant photons in the visible spectrum due to their low optical band gap of 1.25−1.33 eV. The highest photocurrent of −2.0 mA/cm^2 at 0.45 V vs reversible hydrogen electrode (RHE) was recorded for CuO films consisting of six layers under 1 sun illumination. A more porous surface, low charge transfer resistance, and high double-layer capacitance at the CuO/electrolyte interface observed for the films consisting of six layers contributed to the high photocurrent density attained by the films. CuO films consisting of six layers prepared using the conventional two-step heat treatment process for comparative purposes yielded 65.0% less photocurrent at 0.45 V vs RHE compared to similar films fabricated via the three-step heating method. The photocurrent response of the CuO nanostructures prepared using the three-step heat treatment process is promising and can be employed for making CuO for photovoltaic and optoelectronic applications.

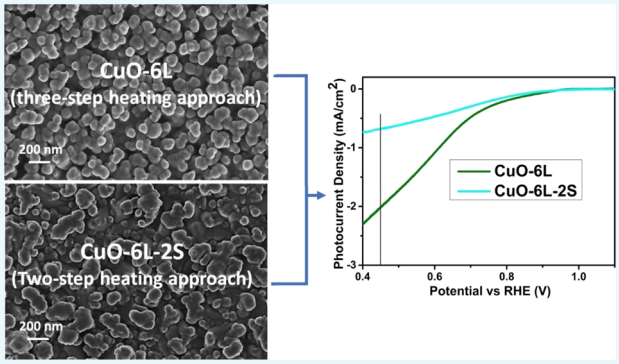

1. INTRODUCTION

Hydrogen (H_2) fuel is a fascinating clean energy alternative owing to its large power density and release of water as a by-product upon oxidation. It can be produced using fossil fuels, coal, natural gas, and renewable sources, among others.[1,2] The renewable methods of producing hydrogen include the gasification of biomass[3] and photocatalysis of water.[4] The photocatalytic approach has attracted much research interest over the years due to the abundance of solar radiation and water; the raw resources needed for the production of hydrogen fuel. Crucial to this approach is a semiconductor material that is capable of capturing a significant portion of the solar radiation to produce electron−hole pairs in a photocatalytic cell, which are then utilized in electrolyzing water to yield H_2. Many semiconductors such as Cu_2O, CuO, and CdS have been investigated for use as photocathodes in the photocatalytic cell for water splitting. The interest in CuO for use as a photocathode in photocatalytic H_2 production is mainly because of its ability to harvest a significant amount of solar radiation in the visible region due to its small band gap of 1.21−1.7 eV.[5,6] Kushwaha et al. prepared CuO nanoleaves and reported a photocurrent density of −1.50 mA/cm^2 at 0 V vs Ag/AgCl after applying the films in photocatalytic water splitting in 0.1 M Na_2SO_4 electrolyte and under 1 sun illumination.[7] Meanwhile, Xia et al. fabricated CuO nanosheets and achieved a maximum photocurrent density of 0.12 mA/cm^2 at 0 V vs Ag/AgCl in a self-powered PEC device for water splitting.[8]

Nanostructured CuO can be prepared using various methods such as electrodeposition,[9] sol−gel,[10] chemical vapor deposition,[11] spray pyrolysis,[12] thermal oxidation,[4] and reactive sputtering.[13] Subjecting the deposited films to different heat treatments to produce CuO nanostructures is one of the key processes common to these methods. This is key because of the significant role that temperature plays in the formation of nanostructured materials and its influence on their properties for photocatalytic applications.[14,15] Among these methods of CuO films preparation, the sol−gel is a cheap and easily scalable approach.

In the sol−gel method, a chemical precursor solution is prepared and deposited onto a substrate followed by heat

Received: July 16, 2021
Accepted: November 15, 2021
Published: December 2, 2021

treatment of the films to produce the nanostructures. The two-step heat treatment process where the first step is employed to dry the deposited films (100−150 °C) and a second step is engaged to calcinate the films at higher temperatures (400−700 °C) has been mostly used for the preparation of CuO films using the sol−gel method.[6,10,16] Another heat treatment process could be introduced in which each layer of the deposited films is treated at temperatures between 230−350 °C immediately after drying. This can result in the layer-by-layer formation of a mixed phase of CuO/Cu_2O nanostructures before calcination to form CuO films.[17,18] The layer-by-layer deposition of nanostructures has been shown to encourage the columnar growth of grains, improving electron mobility and film conductivity[19,20] that are vital for photocatalytic applications. Therefore, the systematic utilization of a three-step heat treatment process for the preparation of CuO films using the sol−gel method in which the deposited films are first treated at two different temperatures before calcination could alter the properties of the films to favor photocatalytic water splitting.

In this research, a three-step heat treatment process was used to prepare CuO nanostructures for photocatalytic hydrogen production. The nanostructured CuO films were prepared on FTO substrates using the sol−gel dip-coating deposition technique. Dip-coated films in 2, 4, 6, 8, and 10 layers were prepared by drying each layer using a two-step method. The films were first dried at 110 °C for 10 min and further treated for 5 min after raising the temperature to 250 °C. The films prepared were annealed at 550 °C for 1 h and allowed to cool naturally to room temperature. The photocatalytic performance of CuO films consisting of six layers produced a maximum photocurrent of −2.0 mA/cm^2 at 0.45 V vs RHE. CuO films consisting of six layers prepared using the conventional two-step heat treatment process (dried at 110 °C and annealed at 550 °C) for comparative purposes yielded the least photocurrent of −0.7 mA/cm^2 at 0.45 V vs RHE. The three-step heat treatment process for preparing CuO nanostructures developed in this study showed a promising photoresponse during photocatalytic water splitting and could be employed for making CuO films for photovoltaic and optoelectronics applications.

2. EXPERIMENTAL SECTION

2.1. Precursor Preparation and Film Deposition. The precursor used for the dip-coating process was obtained by dissolving 0.25 M of copper acetate in 90% propan-2-ol, 10% diethanolamine, and polyethylene glycol 400. The copper acetate salt was poured into propan-2-ol and stirred using a magnetic stirrer for 1 h at room temperature. Diethanolamine was then added to the mixture and further stirred for 1 h. Lastly, polyethylene glycol 400 was added, and the suspension was stirred for an additional 1 h to obtain the precursor used for film deposition.

The FTO substrates used for CuO films deposition were cleaned using acetone, ethanol, and deionized water for 15 min each and dried with nitrogen gas. The FTO substrate was immersed into the prepared precursor solution using a PTL-MM01 dip-coater and withdrawn at the speed of 2 mm/s. The films were first dried on a hot plate at 110 °C for 10 min; the temperature was raised to 250 °C, and the films were further heated at that temperature for 5 min. The same procedure was followed to produce films of 2, 4, 6, 8, and 10 layers, respectively. The films produced were taken into a heating furnace preheated to 300 °C. The temperature of the furnace was then raised to 550 °C at the rate of 10 °C/min, calcined for 1 h, and allowed to naturally cool down to room temperature to obtain CuO films. CuO films consisting of 2, 4, 6, 8, and 10 layers were labeled CuO-2L, CuO-4L, CuO-6L, CuO-8L, and CuO-10L, respectively. Figure 1 presents the diagrammatic illustration of the

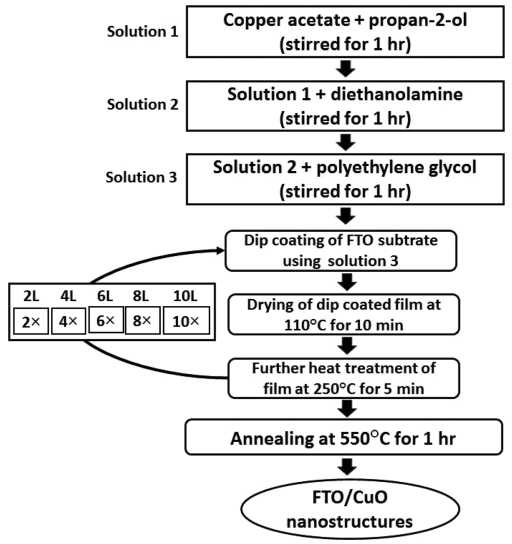

Figure 1. A schematic representation of the procedure used for the preparation of CuO films.

experimental procedure used for the preparation of the CuO films. Additional CuO films were prepared following the same procedure as illustrated in Figure 1, except that a two-step heat treatment process was used where the films were only dried and annealed at 110 and 550 °C, respectively, and labeled as CuO-6L-2S. The films were prepared to compare their structural and photoresponse properties with the films produced via the three-step heat treatment process.

2.2. Characterization. X-ray diffraction (XRD) technique was engaged to study the structural properties of the CuO films using Bruker D2 PHASER-e diffractometer of Cu K_α radiation at 0.15418 nm wavelength. Field-emission gun scanning electron microscopy (FEG-SEM) was performed using the Ultrafast 540 instrument to study the surface morphology of the films and to obtain their cross-sectional images for film thickness estimation. The FEG-SEM instrument was coupled to an energy-dispersive X-ray spectroscopy (EDS) setup, which was used to perform elemental mapping on the CuO film surfaces. The optical absorption of the films was studied using the CARY 100 BIO UV−Vis (UV−visible) spectrometer. Raman spectroscopy investigations were conducted on the films using a Jobin Yvon Horiba TX64000 Raman spectrometer with an Ar excitation laser of 514 nm.

2.3. Electrochemical Measurements. Electrochemical measurements were done using a VersaSTAT 3F potentiostat from Princeton Applied Research attached to the PEC cell. The cell consists of Ag/AgCl in 3 M of KCl, 2 × 2 cm platinum mesh, and the FTO/CuO films as the reference, counter, and working electrodes respectively, and NaOH (pH = 13.6) as the electrolyte. Linear sweep voltammetry (LSV) was conducted on the films under dark and light conditions at the scan rate of 0.05 V/s to determine the photoresponse of the CuO photocathodes. The light source used for the measurements was a Newport Oriel LCS 100 solar simulator under A.M1.5G illumination calibrated to 1 sun intensity with a Newport 91,150 V reference cell. The area of the CuO photocathodes exposed to

https://doi.org/10.1021/acsomega.1c03796
ACS Omega 2021, 6, 33398−33408

light was 0.49 cm^2. Electrochemical impedance spectroscopy (EIS) was done on the photocathodes in the dark at −0.4 V vs Ag/AgCl between 10,000 to 0.1 Hz and with a 10 mV excitation amplitude. The results obtained from the EIS measurements were fitted to an equivalent circuit model using the ZView software. Mott−Schottky (M-S) measurements were conducted on the photocathodes at 1000 Hz, AC potential amplitude of 10 mV, and DC potential range of −0.6 to 0.6 V vs Ag/AgCl in dark conditions. The Nernst relation in eq 1 was engaged in converting all the potential against Ag/AgCl reference to the RHE scale

$$V_{RHE} = 0.1976\ V + (0.059 \times pH) + V_{Ag/AgCl} \quad (1)$$

where V_{RHE} stands for the potential in the RHE reference, 0.1976 V is the estimation that represents the standard potential of Ag/AgCl vs a normal hydrogen electrode (NHE) at 25 °C, and $V_{Ag/AgCl}$ is the potential vs the Ag/AgCl reference electrode used during the electrochemical measurements.[26,27]

3. RESULTS AND DISCUSSION

3.1. Film Properties. *3.1.1. Structural Properties.* Structural properties were extracted from the XRD results of the CuO films presented in Figure 2. The prominent peaks at the $(\bar{1}11)$

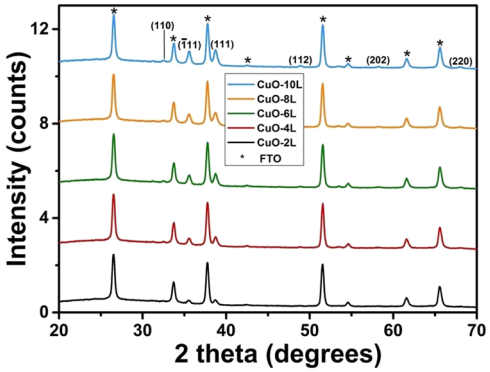

Figure 2. XRD results of CuO films consisting of the different numbers of film layers.

and (111) planes were detected in the XRD patterns of the films, indicating the formation of the tenorite crystal structure of CuO with lattice parameters a = 4.64 Å, b = 3.4 Å, c = 5.09 Å, and β = 99.5° in line with JCPDS no. 05-0661. Other weak peaks of CuO were observed at the (110), (112), (202), and (220) planes. Diffraction peaks of copper (Cu) and other phases of its oxides were not seen in the XRD patterns, implying the synthesis of CuO films of high quality. The intensity of the CuO diffraction peaks increases with the number of deposited layers, which is an indication of increasing film thickness.[21] The Debye−Scherrer method was used to extract the crystal size (D) of the films using the peak at $(\bar{1}11)$ in line with the formula $D = 0.9\lambda/\beta \cos\theta$, where λ is the wavelength, β represents the full width at half maximum, and θ is the diffraction angle. The films revealed crystal sizes in the range of 19.31−20.65 nm. Increasing the film thickness through the deposition of additional film layers and following the three-step heat treatment approach adopted for the CuO preparation did show any effect on their crystal size.

The XRD pattern of sample CuO-6L-2S prepared using the two-step heat treatment process is presented in Figure S1. The films also revealed prominent peaks of CuO at the $(\bar{1}11)$ and (111) planes. Similarly, the Debye−Scherrer method was used to obtain the approximate crystal size (D) of the films. A crystal size value of 16.95 nm was estimated for the films, representing a 12% decrease compared to the values obtained for CuO films prepared using the three-step heat treatment process. A plot of the crystal size values for all the CuO films is presented in Figure 3. Relatively uniform crystal size values were observed for CuO

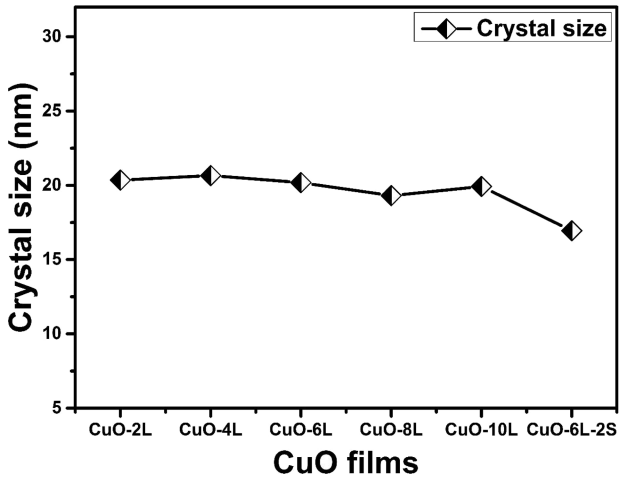

Figure 3. The approximate crystal size values of CuO films.

films prepared using the three-step heat treatment process, which decreases for CuO-6L-2S films fabricated using the two-step heating approach. The increased crystal size recorded for the films prepared using the three-step heating approach is attributed to the layer-by-layer heat treatment of the films at 250 °C. The layer-by-layer deposition of nanostructured films has been shown to improve crystallization, which can consequently enhance photocatalytic capabilities.[19,20]

Raman spectroscopy studies done on the CuO films yielded additional structural information of the films. The results of the Raman spectroscopy measurements performed on the films are given in Figure 4 and reveal the $2B_g$ and $1A_g$ vibrational phonon

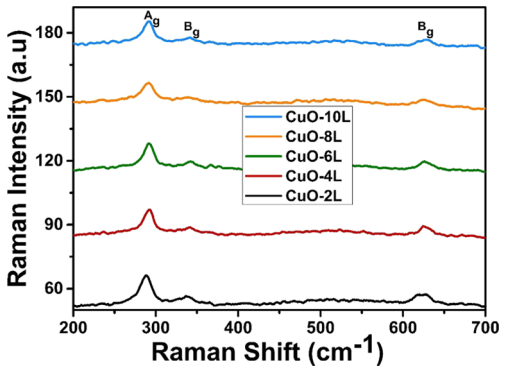

Figure 4. Raman spectra of CuO films consisting of various numbers of film layers prepared using the three-step heat treatment process.

modes for CuO. The Raman peak at 291.8 cm^{-1} is designated to the A_g mode, and the ones at 242.0 and 627.4 cm^{-1} represent the B_g modes.[22] Raman peaks belonging to copper (Cu) or other phases of its oxides were not observed, affirming the high purity of the fabricated CuO films. The intensities of all the Raman active peaks obtained for all the films are similar, which is an indication of similar crystallinity for all the fabricated CuO films.[23] This agrees with XRD analysis, where similar crystal size

https://doi.org/10.1021/acsomega.1c03796
ACS Omega 2021, 6, 33398−33408

values were obtained for all the CuO films prepared using the three-step heating process.

3.1.2. Morphology, Film Thickness, and Elemental Mapping. The surface images obtained from the FE-SEM investigation of the CuO films prepared using the three-step heating process are presented in Figure 5a−e for films with 2, 4, 6, 8, and 10 layers, respectively. The films revealed agglomerated spherical nanoparticles, which are more compact for samples with two layers. The surface of the films became less compact with additional film layers, producing the most porous surface for films consisting of six layers. The grain sizes of the films were not estimated due to the agglomeration of the particles. In photocatalytic water splitting, a porous nanostructured morphology is desirable for improving efficiency because it can promote the separation of photogenerated charge carriers and can provide more active sites for redox reactions during photocatalysis.[24,25] Figure 5f presents the surface morphology of CuO-6L-2S prepared using the two-step heat treatment process. The CuO-6L-2S films appeared to consist of more compact and agglomerated nanoparticles when compared to the surface morphology of CuO-6L films (Figure 5c). This could limit its photocatalytic activity during water splitting.[26−28]

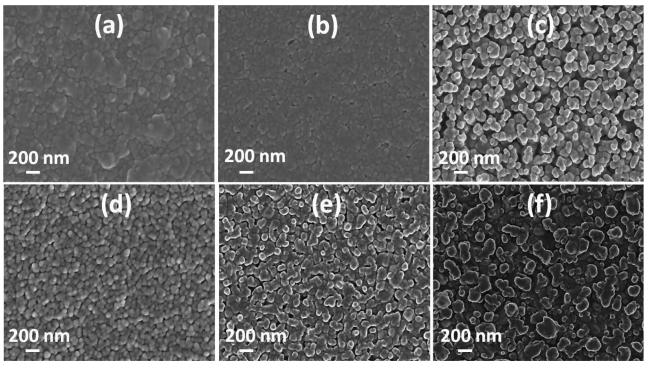

Figure 5. FEG-SEM micrographs of CuO films prepared using the three-step heat treatment process consisting of (a) 2, (b) 4, (c) 6, (d) 8, and (e) 10 layers, respectively. (f) Micrograph of CuO-6L-2S fabricated via the two-step heating approach.

The thicknesses of the CuO films produced were estimated from their cross-sectional views using ImageJ software. Figure 6a,b shows the cross-sectional view of the CuO films consisting of 2 and 10, layers, respectively. The cross-sectional views of all the CuO films prepared using the three-step heating approach are presented in Figure S2, and their estimated thicknesses are shown in Table 1. As expected, the thickness of the films increases with the number of deposited film layers. For efficient light absorption and charge transport, an optimal film thickness will be paramount for achieving better photocatalytic reactions.[9,29]

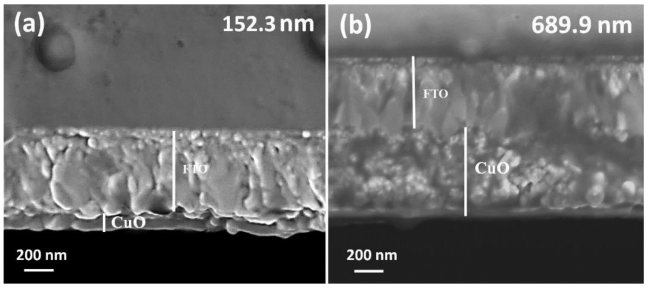

Figure 6. FEG-SEM cross-sectional views of CuO films consisting of (a) 2 and (b) 10 layers, respectively.

Table 1. Film Thickness of Prepared CuO Samples Consisting of Different Film Layers

sample	film thickness (nm)
CuO-2L	142 ± 15
CuO-4L	264 ± 28
CuO-6L	419 ± 37
CuO-8L	543 ± 52
CuO-10L	690 ± 33
CuO-6L-2S	232 ± 36

The film thickness of CuO-6L-2S prepared using the two-step heat treatment process was extracted from the film's cross-sectional view given in Figure S3c and Table 1. The film thickness of the CuO-6L-2S sample was 44.6% less than that of the CuO-6L films prepared using the three-step heating approach despite having the same number of film layers. The single-step drying of Cu precursor deposited on FTO and dried at 110 °C in air was not high enough to result in the formation of some CuO/Cu_2O nanostructures. This may have allowed some of the Cu-based films dried on FTO to dissolve in the precursor solution during the deposition of subsequent layers, leading to the decreased film thickness obtained for CuO-6L-2S films.

Elemental mapping was performed on samples CuO-2L, CuO-6L, and CuO-6L-2S to investigate the distribution of the constituent elements of CuO on the surface of the films. The results are presented in Figure 7 a−c for samples CuO-2L, CuO-6L, and CuO-6L-2S, respectively. The EDS maps show uniform distribution of Cu and O on the surface of the films. Tin (Sn) was also detected in the EDS maps due to the SnO_2 content of the FTO substrates used to deposit the films. More Sn was detected in CuO-2L and CuO-6L-2S samples, as seen in their EDS maps, due to their reduced film thicknesses relative to CuO-6L films (Table 1).

3.1.3. Optical Properties. UV−Vis studies done on the films yielded the absorption spectra and optical band gaps of the CuO nanostructures prepared using the three-step heating approach. Figure 8 presents the absorption spectra of the CuO samples. The films exhibited impressive absorption in the visible spectrum, absorbing significant photons at wavelengths between 400 and 700 nm. Natural solar radiation is estimated to consist of 52% infrared radiation (700−2500 nm), 43% visible light (400−700 nm), and 5% ultraviolet (300−400 nm).[30] Therefore, the absorption region of the CuO films prepared is very desirable for application in photocatalytic hydrogen production. The absorbance of the films increases with the number of layers because of the higher atomic concentration resulting from increasing film thickness.

The Tauc approximation was used to extract the indirect and direct band gaps of the films[22] that are shown in Figure 9a,b. The optical indirect band gap of the CuO films ranges between 1.25−1.33 eV, which was lower than the values reported by several authors for the films.[9,31−33] The low band gap obtained for the CuO films makes them suitable for photocatalytic applications. Before the final heat treatment of the films at 550 °C, each of the film's layers was dried at 110 and 250 °C. Treating each layer at 250 °C is enough for the formation of the CuO/Cu_2O composite nanostructure, which gets oxidized to pure CuO with the third heat treatment at 550 °C. The layer-by-layer deposition of the nanostructured films during the second heat

https://doi.org/10.1021/acsomega.1c03796
ACS Omega 2021, 6, 33398−33408

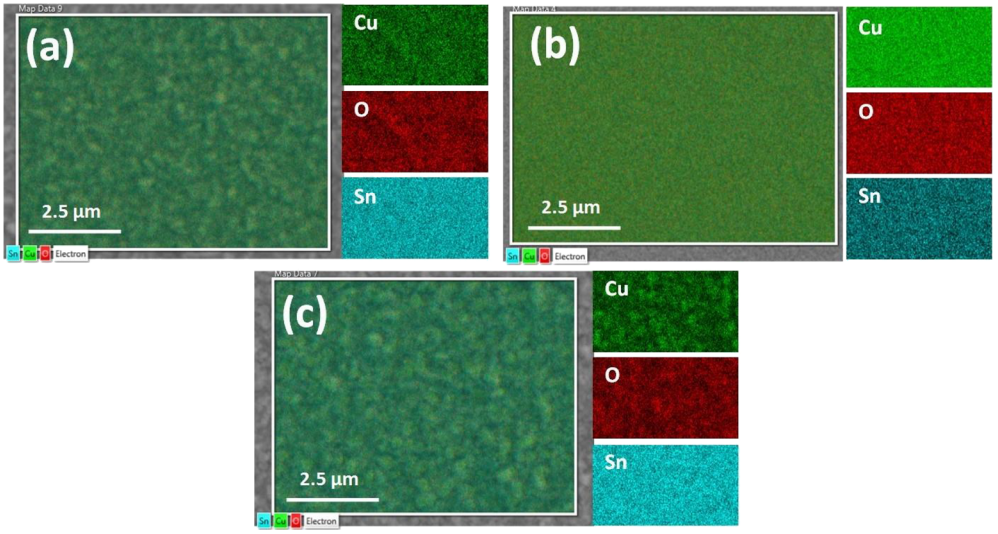

Figure 7. The EDS maps of (a) CuO-2L, (b) CuO-6L, and (c) CuO-6L-2S films, respectively.

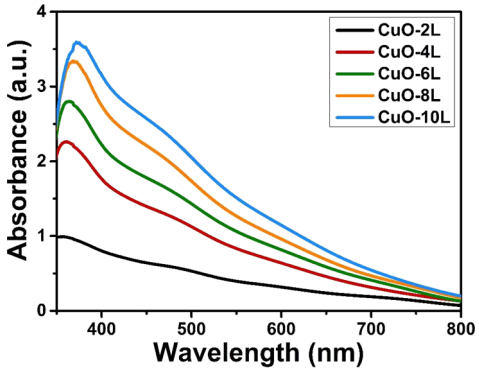

Figure 8. UV−Vis absorption spectra of CuO films consisting of the different numbers of film layers.

treatment process may have encouraged the columnar growth of the grains and improved crystallization. These may have led to a reduction in the number of scattering centers for light and increased its attenuation coefficient, resulting in improvement in light absorption and consequently decreasing the band gap of the CuO films produced.[34] The indirect band gap of 2.18 ± 0.03 was estimated for the CuO films, which was also lower than some reported values in the literature.[32,33]

3.2. Electrochemical Studies. *3.2.1. Photocurrent Density Measurements.* The photocurrent densities of the CuO photocathodes were obtained from the negative linear voltammetry scan conducted on the films in dark and light conditions, and the results are given in Figure 10a for films prepared using the three-step heat treatment process. The least photocurrent value of −1.1 mA/cm^2 at 0.45 V vs RHE was obtained for films with two layers. The low photocurrent is ascribed to the poor light absorption resulting from the limited thickness of the films and the compact nature of the nanoparticles at the film's surface, which caused poor charge separation and reduced photocatalytic efficiency. The maximum photocurrent density of −2.0 mA/cm^2 at 0.45 V vs RHE was attained for films with six layers. The highest photocurrent density attained for the pristine CuO films was well above many photoresponses that have been reported for the films at that potential and illumination condition.[9,25,35−38] Table 2 compares the maximum photocurrent attained by the CuO films in this project with other reported values in the literature. The enhanced photocurrent obtained for the films with six layers in this project is largely related to the porous nature of the film's surface, which created a larger area and increased active sites for water reduction reactions, thus enhancing the photocurrent. In addition, the thickness of the films with six layers may have been optimal for both light absorption and charge separation relative to the other films. A further increase in the number of film layers to 8 and 10, which increases the thickness of the films, resulted in a decreased photocurrent density at 0.45 V vs RHE. The further increase in film thickness enhanced photon absorption (Figure 8) and the number of photogenerated electron−hole pairs.

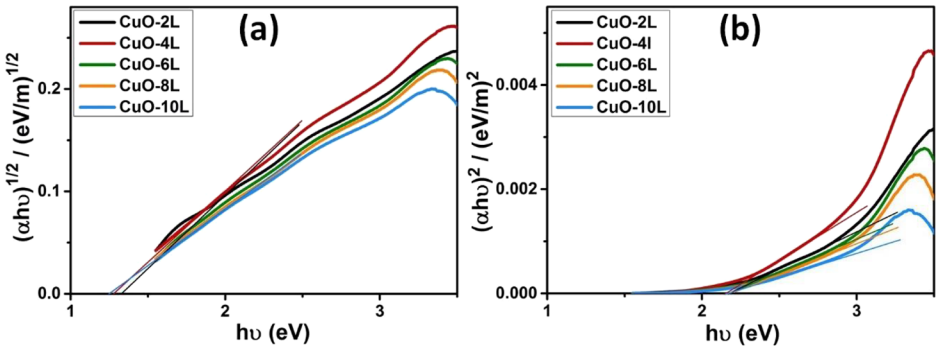

Figure 9. Estimated (a) indirect and (b) direct optical band gaps of the CuO films prepared using the three-step heat treatment process.

https://doi.org/10.1021/acsomega.1c03796
ACS Omega 2021, 6, 33398−33408

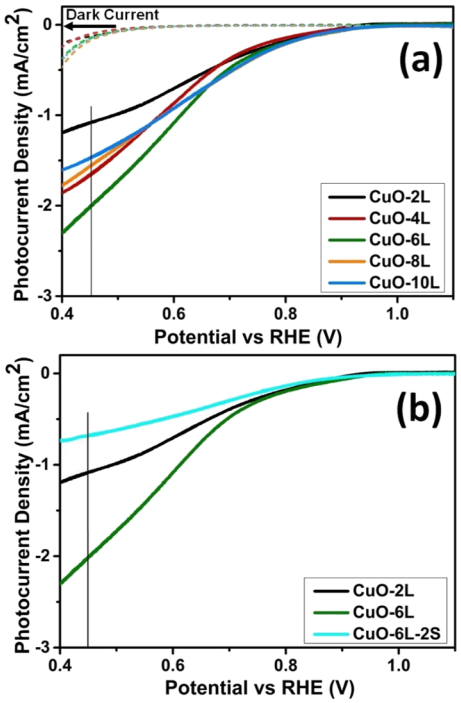

Figure 10. (a) Photocurrent response of CuO photocathodes with the different numbers of film layers prepared using the three-step heat treatment process. (b) Comparison of the photoresponse of CuO-6L-2S fabricated using the two-step heat treatment approach with those of the CuO-6L and CuO-2L films.

However, it did not result in the enhancement of the photocurrent response. This is attributed to two reasons. First, the carrier diffusion length of CuO is about 200 nm,[39] and as a result, the photogenerated charge carriers generated in the bulk of the thicker films may recombine before getting to the surface to contribute to the reduction of water. Secondly, the porosity of films with 8 and 10 film layers appeared to have decreased in comparison to the ones with six layers as seen in their SEM images (Figure 5), which will result in poor charge separation at the surface, thus reducing their photocurrent. All the CuO films had similar onset potential (V_{onset}) for photocurrent at 0.9 V vs RHE, which is more positive than many reported values in other studies[25,35,36] and is an advantage for their application in photocatalysis.[25] The flat band potential that will be discussed in Section 3.2.3 and the open circuit voltage (V_{oc}) combines to determine the V_{onset} of the photocathodes. Larger V_{oc} values are beneficial in reducing the V_{onset} of a photocathode.[40]

The photocurrent density of CuO-6L-2S films prepared using the two-step heat treatment process was measured in order to compare its photoresponse with the ones fabricated using the three-step heating approach. Figure 10b presents a comparison of the photocurrent density of CuO-6L-2S, CuO-6L, and CuO-2L photocathodes. CuO-6L-2S films yielded the least photocurrent of 0.7 mA/cm2 at 0.45 V vs RHE, which was 65.0% less than the value attained by CuO-6L films at the same potential. The thickness of CuO-6L-2S was lower than that of CuO-6L, which may limit its photon absorption and photocatalytic activity.[9,46] However, the photocurrent density obtained for CuO-6L-2S is less than the value achieved for CuO-2L films by 36.4% despite being 63.4% thicker. This confirmed that the films prepared using the three-step heat treatment process (CuO-6L and CuO-2L) yielded superior photo response compared to the ones produced via the two-step heating approach (CuO-6L-2S). The low photocurrent response of CuO-6L-2S is largely associated with two major reasons. First, the surface morphology of the films appeared to be more compact and agglomerated compared to the ones prepared using the three-step heat treatment process (Figure 5) ,which can limit charge separation and photocatalytic activity.[27] Second, the poor crystallization of CuO-6L-2L films compared to the ones prepared using the three-step heating process can limit electron mobility in the films,[19] which will negatively affect their photocatalytic efficiency.

The solar conversion efficiency (η_c) of the CuO films were calculated using eq 2

$$\eta_c(\%) = \frac{J_{ph} \times (1.23 - V_{app})}{P_{in}} \quad (2)$$

where J_{ph} (mA/cm^2) is the measured photocurrent density, V_{app} is the applied potential vs RHE in volts (V), and P_{in} (mW/cm^2) is the input power of the solar radiation.[47,48] The η_c values estimated for the CuO films are given in Figure 11. The highest and lowest η_c values were 1.92 and 0.98% at 0.4 V vs RHE for the CuO films prepared using the three-step heating approach, respectively. The conversion efficiency of CuO-6L-2S films

Table 2. Photocurrent Density (J) Achieved for Different CuO Photocathodes of Different Nanostructures Prepared Using Various Methods

material and morphology	preparation method	photocurrent density (J)	reference
CuO nanoparticles	sol−gel dip-coating	−2.0 mA/cm^2 at 0.45 V vs RHE, 1 M NaOH electrolyte, and under 1 sun	this work
CuO nanowires	facile thermal treatment	−1.4 mA/cm^2 at 0 V vs RHE, 1 M Na_2SO_4 electrolyte, and under 1 sun (100 mW/cm^2)	35
CuO nanoparticles	electrodeposition	−0.49 μA/cm^2 at −0.55 V vs Ag/AgCl, 1 M KOH electrolyte, and 1 sun	36
CuO pyramid structures	electrodeposition	−0.50 mA/cm^2 at 1.23 V vs Ag/AgCl, 0.5 M Na_2SO_4 electrolyte, and under 1 sun	9
CuO nanoparticles	sol−gel dip-coating	−0.94 mA/cm^2 at 0 V vs RHE, 1 M Na_2SO_4 electrolyte, and under 240 mW/cm^2 irradiation	41
CuO intermingled nanosheets	microwave-assisted	−1.15 mA/cm^2 at 0 V vs RHE, 0.1 M Na_2SO_4 electrolyte, and under 1 sun	38
CuO nanoleaves	hydrothermal	−1.50 mA/cm^2 at 0 V vs Ag/AgCl, 0.1 M Na_2SO_4 electrolyte, and under 1 sun	38
CuO nanowires	electrodeposition	−1.40 mA/cm^2 at −0.4 V vs Ag/AgCl, 1 M NaOH electrolyte, and under 320 mW/cm^2 irradiation.	42
CuO nanoparticles	thermal condensation	−0.50 mA/cm^2 at 0 V vs RHE, 0.1 M Na_2SO_4 electrolyte, and under 1 sun.	43
CuO nanoparticles	electrodeposition	−1.39 mA/cm^2 at 0 V vs RHE, 0.1 M Na_2SO_4 electrolyte, and under 1 sun	44
CuO hollow spheres	doctor-blade	−1.47 mA/cm^2 at −0.3 V vs Ag/AgCl, 0.5 M Na_2SO_4 electrolyte, and under 1 sun	45
CuO nanoparticles	sol−gel spin-coating	−0.35 mA/cm^2 at 0.5 V vs RHE, 0.1 M Na_2SO_4 electrolyte, and under 1 sun	29
CuO nanoparticles	sputtering	−1.68 mA/cm^2 at 0 V vs RHE, 0.1 M Na_2SO_4 electrolyte, and under 1 sun	46

https://doi.org/10.1021/acsomega.1c03796
ACS Omega 2021, 6, 33398−33408

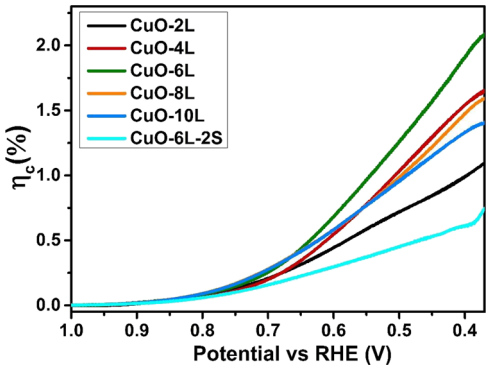

Figure 11. The solar conversion efficiency of CuO films.

prepared using the two-step heat treatment process was 0.61% at 0.4 V vs RHE. This was 68.2 and 37.8% lower than the maximum and minimum values attained by the CuO films fabricated via the three-step heating process at the same potential, respectively.

The proposed energy diagram, band bending, and charge transport mechanism of the CuO films in a photocatalytic cell are illustrated in Figure 12. When a p-type semiconductor is

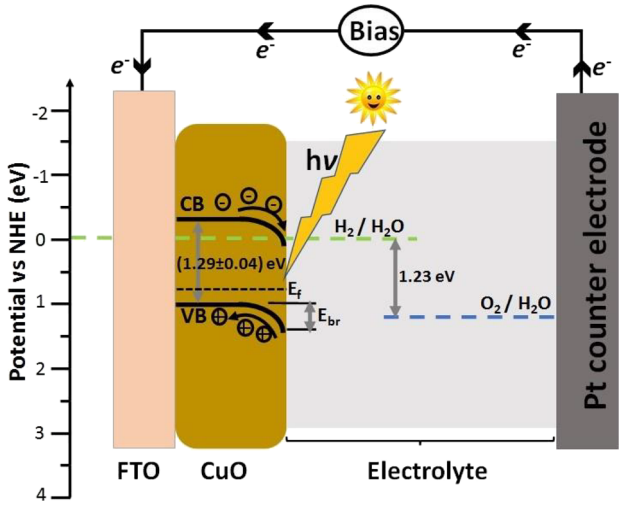

Figure 12. Energy diagram and band bending of CuO films in a photocatalytic cell.

immersed into an electrolyte, the transfer of charges will occur at the surface of the photocathode, resulting in the system attaining an equilibrium state. The majority charge carries, which are holes in this case, will be moved from the CuO films to the oxidized species in the electrolyte. Eventually, the system will attain equilibrium, and a space charge layer will be formed at the surface of the films characterized by the depletion of holes. This will create an electric field in the semiconductor liquid (SCL) region, which will cause the energy bands to bend downward. The band bending will lead to the formation of a potential barrier (E_{br}) against the movement of holes in the photocathode.[49] During photocatalysis, photoexcited electrons in the VB of the photocathode will get driven by the electric field in the SCL to the surface of films to perform the reduction reaction, while the holes are transferred to the FTO back contact.[7]

3.2.2. EIS Analysis. The impedance response of the CuO photocathodes was obtained from their EIS studies performed under dark conditions to understand the charge transport kinetics that happens at the film's surface. The EIS response of the CuO films obtained at 0.6 V vs RHE is represented in the Nyquist plots given in Figure 13, with the inset showing the

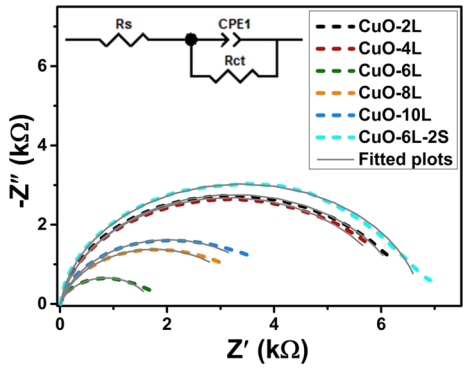

Figure 13. Nyquist plots of the EIS analysis conducted on CuO photocathodes. The dashed colored lines show the raw experimental data, gray solid lines represent the corresponding curves obtained after fitting the raw EIS data with ZView software, and the inset presents the modeled equivalent circuit used in fitting the measured EIS data.

simple Randles circuit used to model the data obtained. In the circuit model, R_s represents the summation of the resistance of the FTO interface, the ionic solution, and the external wires that connect the electrodes to the potentiostat.[50] The constant phase element (CPE) stands for the capacitance at the photoelectrode/liquid interface, also known as the double-layer capacitance, and R_{ct} represents the charge transfer resistance at the CuO/electrolyte interface. The semicircles obtained from the Nyquist plots of the EIS data appeared to be depressed, which is a sign of nonideal capacitance that may arise from the nonuniformity of the CuO film surface.[50,51] Hence, CPE components were utilized to depict the nonideal capacitive response of the films.

The values extracted for the modeled circuit elements after fitting the raw EIS data with ZView is presented in Table 3. Low

Table 3. Approximate Values for Modeled Circuit Elements after Fitting the Raw EIS Data Recorded for the CuO Films Using ZView Software

sample	R_s (Ω)	R_{ct} (kΩ)	CPE (μF)
CuO-2L	11.74	6.49	49.97
CuO-4L	12.66	6.29	66.82
CuO-6L	8.33	1.71	194.66
CuO-8 L	9.75	3.51	182.35
CuO-10L	10.07	4.05	172.4
CuO-6L-2S	12.88	6.76	27.1

series resistance in the range of 8.33−12.88 Ω was obtained for the CuO photocathodes. The CuO films prepared using the three-step heating approach yielded the least resistance to charge transfer of 1.71 kΩ at the CuO/electrolyte interface for films consisting of six layers. This was 3.8 times lower than the value obtained for films consisting of two layers, which recorded the highest resistance among films prepared via the three-step heating process. The compact nature of the grains for films with two layers limited charge separation and is largely responsible for the high R_{ct} experience by the films. The films with six layers had the most porous morphology, which provides a wider surface area for efficient charge separation and more active sites for hydrogen evolution reaction during water splitting. The highest

https://doi.org/10.1021/acsomega.1c03796
ACS Omega 2021, 6, 33398−33408

capacitance at the photocathode/electrolyte interface was observed for CuO films with six layers, while those that consisted of two layers produced the lowest value. High capacitance at the electrode/electrolyte interface enhances the electrode's ability to retain charge carriers at its surface and further reflects the high electrochemical surface area available for water reduction reactions.[52,53] The decreased charge transfer resistance and the high capacitance values at the CuO/electrolyte interface recorded by films with six layers prepared using the three-step heating method are responsible for the high photocurrent density attained by the films.

The CuO-6L-2S films consisting of six layers and prepared using the two-step heating process for comparative purposes yielded higher R_{ct} values and lower double-layer capacitance compared to all the samples prepared via the three-step heating process, as shown in Figure 13 and Table 3. The R_{ct} value obtained for sample CuO-6L-2S is 3.78 times more than the resistance recorded for CuO-6L films prepared via the three-step heating approach. Also, the double-layer capacitance value of 27.1 μF observed for CuO-6L-2S films increased by 7.2-fold when the three-step heating approach was adopted. The high R_{ct} and low capacitance values observed for CuO-6L-2S are responsible for the low photocurrent response attained by the films (Figure 10b). The surface of the CuO-6L-2S films consists of highly compact and agglomerated nanoparticles (Figure 5f), which will limit the surface area and the number of active sites available for hydrogen evolution reaction. This will inhibit charge separation during photocatalysis and increase the R_{ct} at the film's surface, leading to the poor photocatalytic activity observed in the films.

The Bode plots of log |Z| vs log frequency and phase angle against the log frequency of the CuO films are presented in Figure 14a,b. The plot of log |Z| vs log frequency produced the least magnitude of log |Z| for films having six layers prepared using the three-step heating process. A lower log |Z| value implies a drop in the resistance to charge transfer at the junction between the CuO film and the electrolyte, which also explains the high photocurrent response attained by the CuO-6L films. Also, the plot of phase angle vs log frequency showed peaks with the least negative phase angle for CuO-6L films prepared using the three-step heating process. This indicates an improvement in the mobility of charge carriers at the region between the CuO-6L photocathodes and the electrolyte, which is consistent with the observations in Figure 13 and Table 3.[9] The Bode plots for sample CuO-6L-2S prepared using the two-step process for comparative purposes revealed the highest magnitude of log |Z| and the most negative phase angle in the plots of log |Z| vs log frequency and phase vs log frequency, respectively. These results also agree well with the observations made in the Nyquist plots of the films in Figure 13 and the data in Table 3.

3.2.3. Mott–Schottky (M-S) Analysis. The M-S plots obtained from the voltage–capacitance measurements performed on the CuO films prepared using the three-step heating process are presented in Figure 15. The plots exhibited a negative slope for all the CuO photocathodes, affirming their p-type property and justifying the photocathodic current response observed for the films in Figure 10. The flat band potential (V_{fb}) and charge carrier density (N_A) values were deduced from the CuO photocathodes in line with the M-S relation for a p-type material given in eq 3[54]

$$\frac{1}{C^2} = \frac{2}{\varepsilon_0 \varepsilon e A^2 N_A}\left(-V + V_{fb} - \frac{KT}{e}\right) \quad (3)$$

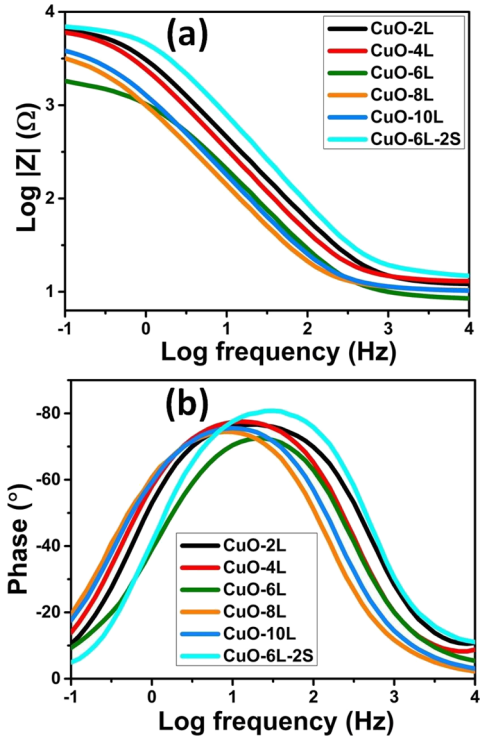

Figure 14. The Bode plots of (a) log |Z| vs log frequency and (b) phase angle vs log frequency obtained from the EIS analysis done on the prepared CuO films.

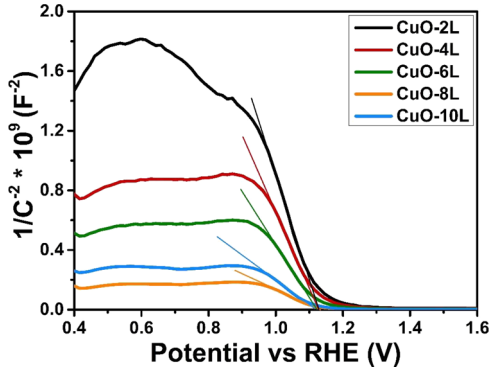

Figure 15. MS plots of CuO films consisting of the different number of film layers; prepared using the three-step heating approach.

where C is the space charge capacitance, e stands for the electronic charge, K is the Boltzmann constant, V is the applied voltage, A is the area of the photocathode's surface, T is the temperature, ε = 18.1 is the dielectric constant for CuO films,[55] and ε_0 is the vacuum permittivity. The N_A values for the photocathodes were extracted from the slope of the MS plots in line with eq 3. Also, the V_{fb} of the CuO films were deduced from the intersection of fitting the linear portion of the MS plots on the potential axis at $1/C^2 = 0$.

The approximate N_A and V_{fb} extracted from the MS plots of the CuO films are given in Table S1. Similar V_{fb} values of 1.144–1.157 V vs RHE were obtained for the CuO films prepared using the three-step heating approach, which explains why identical onset potential for photocurrent was observed for the films (Figure 10). The least charge carrier density of 2.8×10^{20} cm^{-3} was estimated for CuO films consisting of two layers, and the maximum value of 18.1×10^{20} cm^{-3} was obtained for films with

https://doi.org/10.1021/acsomega.1c03796
ACS Omega 2021, 6, 33398–33408

eight layers. Increased charge carrier density can help improve the conductivity of the films and boost photocatalytic efficiency. However, the surface properties of the films can play key roles in determining charge transfer kinetics during photocatalytic reactions. The CuO films prepared are of different thicknesses. This can help in optimizing photon absorption[9] and maximizing the short minority carrier diffusion length of CuO films,[39] which can affect their photocatalytic activity. Therefore, due to the influence of film thickness and surface properties on photocatalytic water splitting, a direct correlation of the charge carrier's density and the photocurrent response of the films was not observed.

3.2.4. Stability. Chronoamperometry measurements were performed on samples CuO-6L and CuO-6L-2S prepared using the three- and two-step heating processes, respectively, at a fixed potential of 0.6 V vs RHE to study the stability of their photocurrent response over time. The results are presented in Figure 16. CuO-6L films were studied because of the high photocurrent response attained by the films. CuO-6L films retained over 56.7 and 51% of their photocurrent density after 200 and 300 s, respectively. CuO-6L-2S exhibited similar photocurrent−time responses with those of CuO-6L, retaining about 53.7 and 47.0% of their photocurrent after 200 and 300 s, respectively. These results are comparable with previous observations made on the stability of pristine CuO films.[35,55] The poor stability exhibited by the films are attributed to the reduction of CuO to Cu_2O by accumulated photogenerated electrons at the film's surface.[35] Cots et al., in their study, retained less than 5% of photocurrent density for pristine CuO photocathodes during photocatalysis and recorded a Faraday efficiency of 45% due to photocorrosion.[42] They attributed the photocurrent density obtained for the films to both photocorrosion and H_2 evolution reaction. In this work, the photocurrent response measured for the CuO films given in Figure 10 are not entirely due to H_2 evolution reaction as part of the observed current may have been due to photocorrosion.[35,42,56] The photogenerated electrons will be more useful for proton reduction to H_2 during photocatalysis if photocorrosion in the films is inhibited. The stability of the CuO films could be improved by the coating of its surface with a thin layer of activated carbon,[57] deposition of a protective layer of a more stable metal oxide such as TiO_2,[41] and surface decoration with a metal such as nickel (Ni).[47] The stability of photoelectrodes in an electrolyte is vital for their application in photocatalytic hydrogen production.[58,59] Therefore, in subsequent studies, it will be important to prioritize enhancing the stability of the CuO films prepared via the three-step heat treatment process by exploring one or more of the possible ways of limiting photocorrosion in the films during photocatalysis.

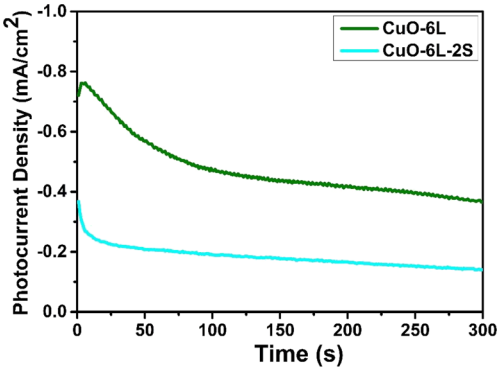

Figure 16. Chronoamperometry study of samples CuO-6L and CuO-6L-2S prepared using the three- and two-step heating approaches, respectively.

4. CONCLUSIONS

Nanostructured CuO films were prepared on FTO using a three-step heat treatment process in a sol−gel dip-coating method. Dip-coated films in 2, 4, 6, 8, and 10 layers were deposited on FTO. Each layer of the deposited films was subjected to a two-step drying approach at 110 and 250 °C for 10 and 5 min, respectively. The films were further treated at 550 °C for 1 h to obtain nanostructured CuO films that were then applied as photocathodes toward photocatalytic water splitting for hydrogen production. The XRD pattern of the films confirmed the tenorite phase of the pure CuO films. Raman spectroscopy revealed the $1A_g$ and $2B_g$ phonon modes of CuO, further confirming the high purity of the films produced. Low optical band gap values ranging between 1.25 and 1.33 eV were estimated for the CuO films, making them suitable for photocatalytic applications. A maximum photocurrent of −2.0 mA/cm^2 at 0.45 V vs RHE was recorded for CuO films consisting of six layers, while the least value of 1.1 mA/cm^2 was observed for films with two layers at the same potential under 100 mW/cm^2 solar irradiance at AM 1.5 G condition. CuO films consisting of six layers prepared using the conventional two-step heat treatment process for comparative purposes yielded 65.0% less photocurrent at 0.45 V vs RHE compared to similar films fabricated via the three-step heating method. CuO films prepared using the three-step heating method and consisting of six layers were more porous compared to the other films as revealed by FE-SEM studies, allowing for easier charge separation of photogenerated charge carriers and leading to the improved photocurrent observed. EIS analysis revealed the least charge transfer resistance at the CuO/electrolyte interface for films consisting of six layers prepared using the three-step heating method, agreeing with the high photocatalytic response achieved for the films. The stability test performed on sample CuO-6L showed that the films could only retain about 56.7% of their photocurrent density after 300 s because of the photocorrosion of the CuO films. Therefore, the photocurrent response measured for the CuO films are not entirely due to H_2 evolution reaction, as part of the observed current may have been due to photocorrosion. Notwithstanding, the three-step heat treatment process for preparing CuO nanostructures developed in this study showed promising photocatalytic response and could also be employed for making CuO films for photovoltaic and optoelectronic applications.

■ ASSOCIATED CONTENT

Supporting Information

The Supporting Information is available free of charge at https://pubs.acs.org/doi/10.1021/acsomega.1c03796.

XRD of CuO films prepared using the two-step heat treatment approach; SEM cross-sectional views of the films; summary of Mott−Schottky analysis data obtained for the films (PDF)

https://doi.org/10.1021/acsomega.1c03796
ACS Omega 2021, 6, 33398−33408

AUTHOR INFORMATION

Corresponding Authors

Pannan I. Kyesmen − *Department of Physics, University of Pretoria, Hatfield 0028, South Africa*; Email: pannan.kyesmen@up.ac.za

Mmantsae Diale − *Department of Physics, University of Pretoria, Hatfield 0028, South Africa*; orcid.org/0000-0002-6035-6688; Email: mmantsae.diale@up.ac.za

Author

Nolwazi Nombona − *Department of Chemistry, University of Pretoria, Hatfield 0028, South Africa*

Complete contact information is available at: https://pubs.acs.org/10.1021/acsomega.1c03796

Notes

The authors declare no competing financial interest.

ACKNOWLEDGMENTS

The authors acknowledge support from the University of Pretoria (UP) and funding from the UP postdoctoral fellowship programme, grant DRI − cost centre A0X816, and the South African Research Chairs Initiative (SARCHI) UID 115463. We acknowledge financial support from NRF N00500, project UID 110983 (Blue Skies Research Program), UID 112085 (NRF Research Development Grant), and the CSIR National Laser Centre Rental Pool Program toward the purchase of the VersaStat 3F potentiostat.

REFERENCES

(1) Chiang, C.-Y.; Aroh, K.; Franson, N.; Satsangi, V. R.; Dass, S.; Ehrman, S. Copper oxide nanoparticle made by flame spray pyrolysis for photoelectrochemical water splitting−Part II. Photoelectrochemical study. *Int. J. Hydrogen Energy* **2011**, *36*, 15519−15526.

(2) Yilanci, A.; Dincer, I.; Ozturk, H. K. A review on solar-hydrogen/fuel cell hybrid energy systems for stationary applications. *Prog. Energy Combust. Sci.* **2009**, *35*, 231−244.

(3) Jeong, Y.-S.; Choi, Y.-K.; Kang, B.-S.; Ryu, J.-H.; Kim, H.-S.; Kang, M.-S.; Ryu, L.-H.; Kim, J.-S. Lab-scale and pilot-scale two-stage gasification of biomass using active carbon for production of hydrogen-rich and low-tar producer gas. *Fuel Process. Technol.* **2020**, *198*, 106240.

(4) Yang, Y.; Xu, D.; Wu, Q.; Diao, P. Cu_2 O/CuO bilayered composite as a high-efficiency photocathode for photoelectrochemical hydrogen evolution reaction. *Sci. Rep.* **2016**, *6*, 35158.

(5) Wang, Z.; Zhang, L.; Schülli, T. U.; Bai, Y.; Monny, S. A.; Du, A.; Wang, L. Identifying Copper Vacancies and Their Role in the CuO Based Photocathode for Water Splitting. *Angew. Chem., Int. Ed.* **2019**, *58*, 17604−17609.

(6) Raship, N.; Sahdan, M.; Adriyanto, F.; Nurfazliana, M.; Bakri, A. In *Effect of annealing temperature on the properties of copper oxide films prepared by dip coating technique*, AIP Conference Proceedings, AIP Publishing, 2017, p 030121.

(7) Kushwaha, A.; Moakhar, R. S.; Goh, G. K.; Dalapati, G. K. Morphologically tailored CuO photocathode using aqueous solution technique for enhanced visible light driven water splitting. *J. Photochem. Photobiol., A* **2017**, *337*, 54−61.

(8) Xia, W.; Luo, M.; Zeng, X.; Yang, J.; Dong, J.; Xu, Q.; Zhang, Z. Different annealing atmosphere gases on the growth and photocurrent performance of CuO films grown on FTO substrate. *ACS Omega* **2018**, *3*, 11354−11361.

(9) Mahmood, A.; Tezcan, F.; Kardaş, G. Photoelectrochemical characteristics of CuO films with different electrodeposition time. *Int. J. Hydrogen Energy* **2017**, *42*, 23268−23275.

(10) Dahrul, M.; Alatas, H. Preparation and optical properties study of CuO thin film as applied solar cell on LAPAN-IPB Satellite. *Procedia Environ. Sci.* **2016**, *33*, 661−667.

(11) Barreca, D.; Comini, E.; Gasparotto, A.; Maccato, C.; Sada, C.; Sberveglieri, G.; Tondello, E. Chemical vapor deposition of copper oxide films and entangled quasi-1D nanoarchitectures as innovative gas sensors. *Sens. Actuators, B* **2009**, *141*, 270−275.

(12) Moumen, A.; Hartiti, B.; Thevenin, P.; Siadat, M. Synthesis and characterization of CuO thin films grown by chemical spray pyrolysis. *Opt. Quantum Electron.* **2017**, *49*, 70.

(13) Patel, M.; Kim, J. Optical and electrical features of semi-transparent CuO photoelectrochemical cell. *Data Br.* **2018**, *17*, 681−688.

(14) Yoon, K. H.; Choi, W. J.; Kang, D. H. Photoelectrochemical properties of copper oxide thin films coated on an n-Si substrate. *Thin Solid Films* **2000**, *372*, 250−256.

(15) Mabrouki, M. Effect of annealing temperature on the structural, physical, chemical, and wetting properties of copper oxide thin films. *Mater. Today: Proc.* **2019**, *13*, 771−776.

(16) Armelao, L.; Barreca, D.; Bertapelle, M.; Bottaro, G.; Sada, C.; Tondello, E. A sol−gel approach to nanophasic copper oxide thin films. *Thin Solid Films* **2003**, *442*, 48−52.

(17) Johan, M. R.; Suan, M. S. M.; Hawari, N. L.; Ching, H. A. Annealing effects on the properties of copper oxide thin films prepared by chemical deposition. *Int. J. Electrochem. Sci.* **2011**, *6*, 6094−6104.

(18) Papadimitropoulos, G.; Vourdas, N.; Vamvakas, V. E.; Davazoglou, D. In *Deposition and characterization of copper oxide thin films*, journal of physics: conference series, IOP Publishing, 2005; p 182.

(19) Schuler, T.; Aegerter, M. A. Optical, electrical and structural properties of sol gel ZnO: Al coatings. *Thin Solid Films* **1999**, *351*, 125−131.

(20) Aegerter, M. A.; Reich, A.; Ganz, D.; Gasparro, G.; Pütz, J.; Krajewski, T. Comparative study of SnO2: Sb transparent conducting films produced by various coating and heat treatment techniques. *J. Non-Cryst. Solids* **1997**, *218*, 123−128.

(21) Braiek, Z.; Gannouni, M.; Assaker, I. B.; Bardaoui, A.; Lamouchi, A.; Brayek, A.; Chtourou, R. Correlation between physical properties and growth mechanism of In2S3 thin films fabricated by electro-deposition technique with different deposition times. *Eur. Phys. J. Appl. Phys.* **2015**, *72*, 10302.

(22) Tran, T. H.; Nguyen, V. T. Copper oxide nanomaterials prepared by solution methods, some properties, and potential applications: a brief review. *Int. Scholarly Res. Not.* **2014**, *2014*, 856592.

(23) Gómez, D. A.; Coello, J.; Maspoch, S. The influence of particle size on the intensity and reproducibility of Raman spectra of compacted samples. *Vib. Spectrosc.* **2019**, *100*, 48−56.

(24) Shen, S.; Jiang, J.; Guo, P.; Guo, L. Facile growth of porous hematite films for photoelectrochemical water splitting. *Int. J. Photoenergy* **2013**, *2013*, 174982.

(25) Basu, M. Porous cupric oxide: efficient photocathode for photoelectrochemical water splitting. *ChemPhotoChem* **2019**, *3*, 1254−1262.

(26) Liu, Y.; Xie, L.; Li, Y.; Yang, R.; Qu, J.; Li, Y.; Li, X. Synthesis and high photocatalytic hydrogen production of SrTiO3 nanoparticles from water splitting under UV irradiation. *J. Power Sources* **2008**, *183*, 701−707.

(27) Nasir, J. A.; ur Rehman, Z.; Shah, S. N. A.; Khan, A.; Butler, I. S.; Catlow, C. R. A. Recent developments and perspectives in CdS-based photocatalysts for water splitting. *J. Mater. Chem. A* **2020**, *8*, 20752−20780.

(28) Pellegrino, F.; Pellutiè, L.; Sordello, F.; Minero, C.; Ortel, E.; Hodoroaba, V.-D.; Maurino, V. Influence of agglomeration and aggregation on the photocatalytic activity of TiO_2 nanoparticles. *Appl. Catal., B* **2017**, *216*, 80−87.

(29) Lim, Y.-F.; Chua, C. S.; Lee, C. J. J.; Chi, D. Sol−gel deposited Cu 2 O and CuO thin films for photocatalytic water splitting. *Phys. Chem. Chem. Phys.* **2014**, *16*, 25928−25934.

(30) Kolås, T.; Røyset, A.; Grandcolas, M.; ten Cate, M.; Lacau, A. Cool coatings with high near infrared transmittance for coil coated aluminium. *Sol. Energy Mater. Sol. Cells* **2019**, *196*, 94−104.

(31) Chaudhary, Y. S.; Agrawal, A.; Shrivastav, R.; Satsangi, V. R.; Dass, S. A study on the photoelectrochemical properties of copper oxide thin films. *Int. J. Hydrogen Energy* **2004**, *29*, 131−134.
(32) Lim, Y.-F.; Choi, J. J.; Hanrath, T. Facile synthesis of colloidal CuO nanocrystals for light-harvesting applications. *J. Nanomater.* **2012**, *2012*, 4.
(33) Das, S.; Alford, T. Structural and optical properties of Ag-doped copper oxide thin films on polyethylene napthalate substrate prepared by low temperature microwave annealing. *J. Appl. Phys.* **2013**, *113*, 244905.
(34) Baikov, M.; Ponyavina, A.; Prishivalko, A.; Sviridov, V.; Sil'Vanovich, N. Effect of the microstructure of closely packed ultradisperse hematite layers on their spectral properties. *J. Appl. Spectrosc.* **1996**, *63*, 297−303.
(35) Li, J.; Jin, X.; Li, R.; Zhao, Y.; Wang, X.; Liu, X.; Jiao, H. Copper oxide nanowires for efficient photoelectrochemical water splitting. *Appl. Catal., B* **2019**, *240*, 1−8.
(36) Xing, H.; Lei, E.; Guo, Z.; Zhao, D.; Liu, Z. Enhancement in the charge transport and photocorrosion stability of CuO photocathode: the synergistic effect of spatially separated dual-cocatalysts and pn heterojunction. *Chem. Eng. J.* **2020**, 124907.
(37) Dalapati, G. K.; Masudy-Panah, S.; Moakhar, R. S.; Chakrabortty, S.; Ghosh, S.; Kushwaha, A.; Katal, R.; Chua, C. S.; Xiao, G.; Tripathy, S.; Ramakrishna, S. Nanoengineered Advanced Materials for Enabling Hydrogen Economy: Functionalized Graphene−Incorporated Cupric Oxide Catalyst for Efficient Solar Hydrogen Production. *Global Challenges* **2020**, *4*, 1900087.
(38) Moakhar, R. S.; Soleimani, F.; Goudarzi, A.; Sadrnezhaad, S. K. A Novel Method to Fabricate Hierarchical Copper Oxide Photoelectrode and Its Application for Photoelectrochemical Water Splitting. *ECS Trans.* **2020**, *97*, 845.
(39) Dasineh Khiavi, N.; Katal, R.; Kholghi Eshkalak, S.; Masudy-Panah, S.; Ramakrishna, S.; Jiangyong, H. Visible Light Driven Heterojunction Photocatalyst of CuO−Cu2O Thin Films for Photocatalytic Degradation of Organic Pollutants. *Nanomaterials* **2019**, *9*, 1011.
(40) Kuang, Y.; Yamada, T.; Domen, K. Surface and interface engineering for photoelectrochemical water oxidation. *Joule* **2017**, *1*, 290−305.
(41) Toupin, J.; Strubb, H.; Kressman, S.; Artero, V.; Krins, N.; Laberty-Robert, C. CuO photoelectrodes synthesized by the sol−gel method for water splitting. *J. Sol-Gel Sci. Technol.* **2019**, *89*, 255−263.
(42) Cots, A.; Bonete, P.; Gómez, R. Improving the stability and efficiency of CuO photocathodes for solar hydrogen production through modification with iron. *ACS Appl. Mater. Interfaces* **2018**, *10*, 26348−26356.
(43) Bae, H.; Burungale, V.; Na, W.; Rho, H.; Kang, S. H.; Ryu, S.-W.; Ha, J.-S. Nanostructured CuO with a thin gC 3 N 4 layer as a highly efficient photocathode for solar water splitting. *RSC Adv.* **2021**, *11*, 16083−16089.
(44) Zhang, Q.; Zhai, B.; Lin, Z.; Zhao, X.; Diao, P. CuO/CuBi2O4 bilayered heterojunction as an efficient photocathode for photoelectrochemical hydrogen evolution reaction. *Int. J. Hydrogen Energy* **2021**, *46*, 11607−11620.
(45) Choi, Y.-H.; Kim, D.-H.; Han, H. S.; Shin, S.; Hong, S.-H.; Hong, K. S. Direct printing synthesis of self-organized copper oxide hollow spheres on a substrate using copper (II) complex ink: Gas sensing and photoelectrochemical properties. *Langmuir* **2014**, *30*, 700−709.
(46) Masudy-Panah, S.; Moakhar, R. S.; Chua, C. S.; Kushwaha, A.; Wong, T. I.; Dalapati, G. K. Rapid thermal annealing assisted stability and efficiency enhancement in a sputter deposited CuO photocathode. *RSC Adv.* **2016**, *6*, 29383−29390.
(47) Dubale, A. A.; Pan, C.-J.; Tamirat, A. G.; Chen, H.-M.; Su, W.-N.; Chen, C.-H.; Rick, J.; Ayele, D. W.; Aragaw, B. A.; Lee, J.-F.; Yang, Y. W.; Hwang, B. J. Heterostructured Cu_2 O/CuO decorated with nickel as a highly efficient photocathode for photoelectrochemical water reduction. *J. Mater. Chem. A* **2015**, *3*, 12482−12499.
(48) Singh, A. K.; Sarkar, D. A facile approach for preparing densely-packed individual p-NiO/n-Fe_2O_3 heterojunction nanowires for photoelectrochemical water splitting. *Nanoscale* **2018**, *10*, 13130−13139.
(49) Kusmierek, E. Semiconductor electrode materials applied in photoelectrocatalytic wastewater treatment—an overview. *Catalysts* **2020**, *10*, 439.
(50) Zhao, Y.; Guan, J.; Liu, F.; Cheng, C.; Zhao, J. Effect of Surface Fe-Sn Intermetallics on Oxide Films Formation of Stainless Steel in High Temperature Water. *High Temp. Mater. Processes* **2018**, *37*, 387−395.
(51) Perini, N.; Prado, A.; Sad, C.; Castro, E.; Freitas, M. Electrochemical impedance spectroscopy for in situ petroleum analysis and water-in-oil emulsion characterization. *Fuel* **2012**, *91*, 224−228.
(52) Jung, S.; McCrory, C. C.; Ferrer, I. M.; Peters, J. C.; Jaramillo, T. F. Benchmarking nanoparticulate metal oxide electrocatalysts for the alkaline water oxidation reaction. *J. Mater. Chem. A* **2016**, *4*, 3068−3076.
(53) Behara, D. K.; Ummireddi, A. K.; Aragonda, V.; Gupta, P. K.; Pala, R. G. S.; Sivakumar, S. Coupled optical absorption, charge carrier separation, and surface electrochemistry in surface disordered/hydrogenated TiO 2 for enhanced PEC water splitting reaction. *Phys. Chem. Chem. Phys.* **2016**, *18*, 8364−8377.
(54) Sahoo, P. P.; Zoellner, B.; Maggard, P. A. Optical, electronic, and photoelectrochemical properties of the p-type Cu 3− x VO 4 semiconductor. *J. Mater. Chem. A* **2015**, *3*, 4501−4509.
(55) Patel, M.; Pati, R.; Marathey, P.; Kim, J.; Mukhopadhyay, I.; Ray, A. Highly photoactive and photo-stable spray pyrolyzed tenorite CuO thin films for photoelectrochemical energy conversion. *J. Electrochem. Soc.* **2016**, *163*, H1195.
(56) Emin, S.; Abdi, F.; Fanetti, M.; Peng, W.; Smith, W.; Sivula, K.; Dam, B.; Valant, M. A novel approach for the preparation of textured CuO thin films from electrodeposited CuCl and CuBr. *J. Electroanal. Chem.* **2014**, *717*, 243−249.
(57) Kunturu, P. P.; Huskens, J. Efficient Solar Water Splitting Photocathodes Comprising a Copper Oxide Heterostructure Protected by a Thin Carbon Layer. *ACS Appl. Energy Mater.* **2019**, *2*, 7850−7860.
(58) Afroz, K.; Moniruddin, M.; Bakranov, N.; Kudaibergenov, S.; Nuraje, N. A heterojunction strategy to improve the visible light sensitive water splitting performance of photocatalytic materials. *J. Mater. Chem. A* **2018**, *6*, 21696−21718.
(59) Tawfik, W. Z.; Hassan, M. A.; Johar, M. A.; Ryu, S.-W.; Lee, J. K. Highly conversion efficiency of solar water splitting over p-Cu2O/ZnO photocatalyst grown on a metallic substrate. *J. Catal.* **2019**, *374*, 276−283.

https://doi.org/10.1021/acsomega.1c03796
ACS Omega 2021, 6, 33398−33408